HEFAT2014
10th International Conference on Heat Transfer, Fluid Mechanics and Thermodynamics
14 – 16 July 2014
Orlando, Florida

CONVECTIVE PERFORMANCE OF ENCAPSULATED PHASE CHANGE MATERIAL SLURRIES OF WATER, PAO AND ENGINE OIL IN MICROCHANNELS

Peijie Li and Sarada Kuravi*
*Author for correspondence
Department of Mechanical and Aeronautical Engineering,
Florida Institute of Technology,
Melbourne, 32901, Florida,
The United States
E-mail: pli2012@myfit.edu, skuravi@fit.edu

ABSTRACT

The performance of microencapsulated phase change material slurries of different base fluids inside microchannels is numerically investigated. The presence of phase change material increases the heat capacity of the fluid during melting. For the study, water, polyalphaolefin (PAO) and engine oil have been used as base liquids and n-octadecane has been used as phase change material and the performance at different concentrations flow parameters is analyzed. A microchannel of 600µm hydraulic diameter and 1 cm length was considered for the study and the 3D numerical simulations were performed using COMSOL. For the study, a heat flux of 50 W/cm^2 is used for lower mass flow rate and 500 W/cm^2 is used large mass flow rate. Effective heat capacity method was used to simulate the phase change behavior of PCM. Bulk properties of slurry were used assuming homogeneous distribution of PCM particles. The inlet temperature of the fluid was assumed to be at the 23 ^{0}C and the melting range of PCM is assumed to be 10 ^{0}C. The pressure drop and heat transfer characteristics were simulated and the comparison results for different cases are presented. It was found that the performance of the slurry was higher compared to its base fluid only under certain conditions.

INTRODUCTION

With their steadily increasing heat loads and heat fluxes, current high power density electronics and semiconductor devices, require thermal solutions that go beyond the traditional electronic heat sinks that perform at a higher level. Heat sinks with mini and microchannels are one of the methodologies that are employed for thermal management of these systems. In a minichannel, the channel dimensions may range between 200 µm to 3 mm and in microchannels, the channel dimensions may range between 50 µm to 200 µm. Microchannel heat sinks with their compact design (that enables the heat to be efficiently carried from the substrate into the coolant because of its inherently small passageways) and very large surface-to-volume ratio are capable to remove heat fluxes as high as 1000 W/cm^2 [1]. The typical lengths of traditional microchannels (TM) are 1cm to 2 cm (Figure 1). However, due to high heat flux conditions, the temperature variation along the heat source may be large. In order to maintain isothermality, the mass flow rates are increased, which leads to considerable pressure drop. In applications where high temperature variation and large pressure drop are unacceptable, manifold microchannel heat sink (MMC) [2,3] is shown to be an effective way in reducing the pressure drop and significantly reducing the temperature variation. The MMC heat sink features many inlet and outlet channels alternating at a periodic distance (~ 1mm) along the length of the MMC (Fig. 1). The flow enters the microchannels from the manifold inlet channel, splits and flows through the microchannels, then exits to the manifold outlet channel. This pattern is repeated along the length of the MMC.

The performance of the heat sinks can be improved by utilizing advanced heat transfer fluids such as encapsulated phase change slurries (e.g., [4-7]), nanofluids with metallic particles etc., [8] or by changing surface patterns of walls such as wavy channels (e.g., [9-11]). Researchers have also investigated liquid metals to improve the heat sink performance, due to their high thermal conductivity [12-16].

Encapsulated phase change (EPCM) slurry is a two-phase fluid with a base fluid and micro or nano-sized particles (comprising of phase change material encapsulated in a polymer shell). Due to the presence of PCM in the slurry, the specific heat of the fluid increases when operating in the melting range. In the present study, numerical investigation was performed to analyze the performance of EPCM slurry with different base fluids and compared with that of the single phase liquid.

Many researchers have studied both experimentally and numerically the heat transfer capability of PCM slurry with different base fluids. Some of the references are [4-7, 16-29]. Most of these analyses assume homogeneous and

hydrodynamically fully developed flow. In current study, performance of encapsulated phase change material slurry in a traditional microchannel is investigated and compared to that of single-phase fluid. Three different base fluids (water, engine oil and polyalphaolefin (PAO)), with different particle volume concentrations (0.1, 0.2, and 0.25) were used. PAO is a dielectric oil used in cooling of military avionics systems and is inexpensive and stable. In the current study, the mass flow rate was chosen in order to maintain thermally developing region for all the cases. It was found that for constant mass flow rate, though the thermal performance (heat transfer coefficient improvement) of slurry was found to be better than the base fluid, the increase in viscosity resulted in decreased overall performance (comparison of heat transfer improvement and pressure drop increase).

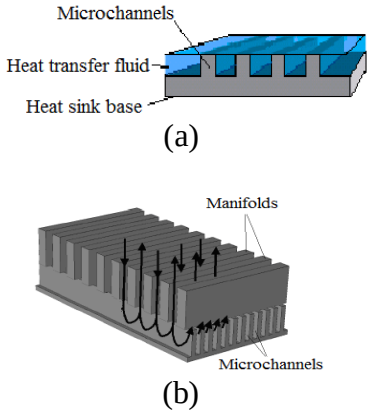

Figure 1 (a) Traditional microchannel heat sink (b) Manifold microchannel heat sink (length~1-2mm)

NOMENCLATURE

A_b	[m^2]	Area of channel base
c	[-]	Volume concentration of slurry
c_m	[-]	Mass concentration of slurry or loading fraction
C_p	[J/kgK]	Specific heat
$C_{p,bulk,1}$	[J/kgK]	Numerical specific heat of bulk fluid
$C_{p,bulk,2}$	[J/kgK]	Theoretical specific heat of bulk fluid
$C_{p,f}$	[J/kgK]	Specific heat of base fluid
$C_{p,p}$	[J/kgK]	Specific heat of EPCM particles
$C_{p,pcm}$	[J/kgK]	Specific heat of PCM
D_h	[m]	Hydraulic diameter
e	[1/s]	Magnitude of shear rate
h	[W/m_2K]	Heat transfer coefficient
h_{sf}	[J/kg]	Latent heat of fusion of PCM
Gz	[-]	Graetz number
H	[m]	Height of the channel or tube
k	[W/mK]	Thermal conductivity
k_{bulk}	[W/mK]	Thermal conductivity of bulk fluid
k_{eff}	[W/mK]	Effective thermal conductivity of bulk fluid
k_{fluid}	[W/mK]	Thermal conductivity of fluid
k_p	[W/mK]	Thermal conductivity of EPCM particle
k_{pcm}	[W/mK]	Thermal conductivity of PCM
L	[m]	Length of the channel
Le_D	[m]	Hydrodynamic entrance length
Le_T	[m]	Thermal entrance length
$\dot{m}$	[kg/s]	Mass flow rate
m_w	[m]	Total thickness of wall and channel, $W+2t_w$
Nu	[-]	Nusselt number
p	[Pa]	Pressure
PF	[-]	Performance factor, $(h/h_{slurry})/(\Delta p_f/\Delta p_{slurry})$
Pr	[-]	Prandtl number
Q	[W]	Heat supply
q	[W/cm^2]	Heat flux
Re	[-]	Reynolds number
T	[K]	Temperature
T_1	[K]	Lower melting temperature
T_2	[K]	Higher melting temperature
T_m	[K]	Average melting temperature = $(T_1+T_2)/2$
T_{Mr}	[K]	Melting range = T_2-T_1
T_{in}	[K]	Temperature at microchannel inlet
T_{out}	[K]	Temperature at microchannel outlet
$T_{wall,max}$	[K]	Maximum wall temperature
t_w	[m]	Thickness of channel wall
t_{base}	[m]	Height of microchannel base
u_{in}	[m/s]	Inlet Velocity
u_{out}	[m/s]	Outlet Velocity
W	[m]	Channel thickness
Δp	[Pa]	Pressure drop, $p_{in}-p_{out}$
ΔT_{bulk}	[T]	Bulk temperature rise, $T_{out}-T_{in}$
α_f	[m^2/s]	Thermal diffusivity of pure fluid
α_{slurry}	[m^2/s]	Thermal diffusivity of slurry
ρ_f	[kg/m^3]	Density of base fluid
ρ_{slurry}	[kg/m^3]	Density of slurry
μ_f	[Pa.s]	Dynamic viscosity of base fluid
μ_{slurry}	[Pa.s]	Dynamic viscosity of slurry

Subscripts

b	Channel base
$bulk$	Bulk
f	Base fluid
in	Inlet
out	Outlet
m	Mean
max	Maximum
p	Particle
pcm	PCM
$slurry$	Slurry
w	Wall

NUMERICAL MODEL

Figure 2 shows the schematic of the microchannel used for simulation and the dimensions represented in the schematic are shown in Table 1. Only half of the channel was considered for simulation because of symmetry.

A. Assumptions

All three fluids are assumed to have constant properties. A constant heat flux was supplied on the wall. The following assumptions are used for the study.

i. Flow is steady and laminar.
ii. Particle concentrations used for the current study range from 0 to 0.25 and hence the fluid can be considered Newtonian [24].
iii. The particle distribution is homogeneous so that the bulk properties are assumed constant except heat capacity, which is a function of temperature.
iv. The melting inside EPCM particles takes place over a range of temperatures, between T_1 and T_2.

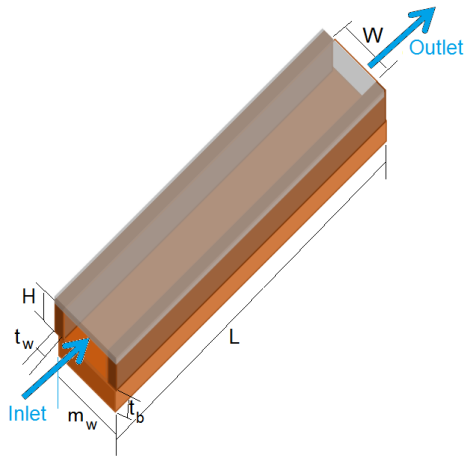

Figure 2 3D schematic flow domain

v. The particles are assumed to follow the fluid without any lag i.e., the difference in the particle and fluid velocities is negligible [7].
vi. There is no temperature gradient inside the particle or the particle melts instantaneously and there is no delay in absorption of heat inside the particle [7].
vii. The effect of particle depletion layer is negligible [30, 31].
viii. The shape of the encapsulated particles is spherical.
ix. Brownian motion can be neglected for the high velocities used [32].

Table 1 Channel dimensions used

Parameter	Value	Units	Descriptions
H	750	µm	Channel height
L	0.25, 0.5, 0.75, 1	cm	Channel length
W	500	µm	Channel width
t_{base}	150	µm	Height of channel base
t_w	150	µm	Thickness of channel wall
m_w	800	µm	$W+2t_w$
D_h	600	µm	Hydraulic diameter

B. Governing equations

The governing equations are as follows:

(a) The mass and momentum equations for the fluid inside the simulation domain can be written as:

$$\frac{\partial u}{\partial x}+\frac{\partial v}{\partial y}+\frac{\partial w}{\partial z}=0 \quad (1)$$

$$\rho\left\{u\frac{\partial u}{\partial x}+v\frac{\partial u}{\partial y}+w\frac{\partial u}{\partial z}\right\}=-\frac{dp}{dx}+\mu\frac{\partial^2 u}{\partial x^2}+\mu\frac{\partial^2 u}{\partial y^2}+\mu\frac{\partial^2 u}{\partial z^2} \quad (2)$$

$$\rho\left\{u\frac{\partial v}{\partial x}+v\frac{\partial v}{\partial y}+w\frac{\partial v}{\partial z}\right\}=-\frac{dp}{dx}+\mu\frac{\partial^2 v}{\partial x^2}+\mu\frac{\partial^2 v}{\partial y^2}+\mu\frac{\partial^2 v}{\partial z^2} \quad (3)$$

$$\rho\left\{u\frac{\partial w}{\partial x}+v\frac{\partial w}{\partial y}+w\frac{\partial w}{\partial z}\right\}=-\frac{dp}{dx}+\mu\frac{\partial^2 w}{\partial x^2}+\mu\frac{\partial^2 w}{\partial y^2}+\mu\frac{\partial^2 w}{\partial z^2} \quad (4)$$

(b) Energy equation for the microchannel wall/fin is:

$$\frac{\partial^2 T_w}{\partial x^2}+\frac{\partial^2 T_w}{\partial y^2}+\frac{\partial^2 T_w}{\partial z^2}=0 \quad (5)$$

(c) The energy equation for the bulk fluid is given below:

$$\rho C_p\left(u\frac{\partial T}{\partial x}+v\frac{\partial T}{\partial y}+w\frac{\partial T}{\partial z}\right)=\frac{\partial}{\partial x}\left(k\frac{\partial T}{\partial x}\right)+\frac{\partial}{\partial y}\left(k\frac{\partial T}{\partial y}\right)+\frac{\partial}{\partial z}\left(k\frac{\partial T}{\partial z}\right) \quad (6)$$

C. Boundary conditions

(a) For flow inside the microchannel

$u = 0$ at the walls (7)

p = p0, atmospheric pressure at the outlet (8)

$u = (\,|\,u\,|\,, 0, 0)$ at the inlet (9)

(b) The boundary conditions for the heat transfer equations are as follows:

For the wall:

$q.n = q_w$; constant heat flux at the base of the fin (10)

$q.n = 0$; adiabatic at symmetry plane and top plate (11)

For the fluid:

$T = T_{in}$ at the inlet (12)

$q.n = (\rho c_p u T).n$; which is the convective heat flux boundary condition at the outlet/exit, (13)

For wall and liquid interface:

T_w = T; continuity of temperature (14)

$-k_w\frac{\partial T_w}{\partial n}=-k_f\frac{\partial T_f}{\partial n}$; continuity of heat flux (15)

D. Slurry Properties

(a) Density: The bulk density of the slurry can be calculated by equation (16), using, c, the volume concentration and the density of PCM:

$$\rho_{bulk}=\rho_{pcm}c+(1-c)\rho_f \quad (16)$$

For calculating the PCM particle density, both the densities of the PCM and shell material and their volume fractions were used, where the PCM average volume fraction in the particle is assumed to be around 90% [4].

(b) Dynamic viscosity: The slurry viscosity is calculated by equation (17) as proposed by Vand [33, 34]:

$$\mu_{bulk} = \mu_f(1 - c - 1.16c^2)^{-2.5} \quad (17)$$

(c) Heat Capacity: The specific heat of the slurry can be calculated by equation (18) [26, 36]:

$$c_{p,bulk} = c_m c_{p,p} + (1 - c_m)C_{p,f} \quad (18)$$

where c_m is the mass concentration, which can be determined by the density of PCM and bulk density of slurry as shown in equation (19)

$$c_m = c\frac{\rho_{pcm}}{\rho_{bulk}} \quad (19)$$

$c_{p,p}$ is the specific heat of EPCM particles and is equal to $c_{p,pcm}$ when the temperature of the particle is outside of the melting range. When the temperature of the particle is within the melting range, sine profile as shown in Figure 3 and described by equation 20 [26] can be used for the specific heat of the particle. The specific heat of solid and liquid phases of PCM is assumed equal in the equation.

$$c_{p,p} = c_{p,pcm} + \left\{\frac{\pi}{2}.\left(\frac{h_{sf}}{T_{Mr}} - c_{p,pcm}\right).\sin\pi\left[\frac{(T - T_1)}{T_{Mr}}\right]\right\} \quad (20)$$

The maximum value of the specific heat during phase change is attained when the temperature of the slurry is in the melting range.

(d) Thermal conductivity: The bulk thermal conductivity of the slurry suspension can be calculated as follows [26]:

$$k_{bulk} = k_f \frac{2 + \frac{k_{pcm}}{k_f} + 2c\left(\frac{k_{pcm}}{k_f} - 1\right)}{2 + \frac{k_{pcm}}{k_f} - c\left(\frac{k_{pcm}}{k_f} - 1\right)} \quad (21)$$

The effective thermal conductivity of slurries in flow is enhanced due to the particle motions and particle-fluid interactions. It can be evaluated as follows:

$$k_{eff} = f.k_b \quad (22)$$

$$\begin{cases} f = 1 + BcPe_p^m \\ B = 0, \quad m = 1.5, \quad Pe_p < 0.67 \\ B = 1.8 \quad m = 0.18 \quad 0.67 \le Pe_p \le 250 \\ B = 3.0, \quad m = \frac{1}{11}, \quad Pe_p > 250 \end{cases}$$

where the particle Peclet number is defined as,

$$Pe_p = \frac{ed_p^2}{\alpha_f} \quad (23)$$

Since the velocity is not fully developed in the current analysis, the shear rate is a function of all the spatial coordinates and corresponding velocities. The magnitude of the shear rate, e can be calculated using the following equation:

$$e = \left(\frac{1}{2}\sum_i\sum_j \gamma_{ij}\gamma_{ji}\right)^{1/2} \quad (24)$$

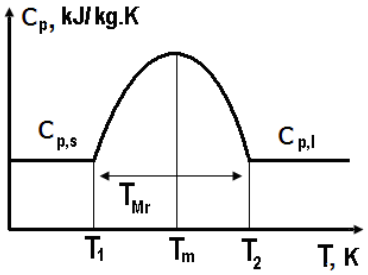

Figure 3 Specific heat of encapsulated PCM, function of temperature [4]

where γ is the shear rate.

STUDY PARAMETERS

The base fluids used for the study are water, oil and polyalphaolefin (PAO) and n-eicosane was assumed as the PCM. Table 2 shows the thermophysical properties of the base fluids and the PCM used in the study.

Table 2 Properties of base fluids

	Water	Oil	PAO	PCM particle
Density (kg/m^3)	997	865	783	774
Specific heat (J/kg.K)	4180	1880	2240	2180
Thermal conductivity (W/m.K)	0.604	0.145	0.143	0.15
Viscosity (Pa.s)	0.001	0.837	0.00445	-
Latent heat (J/kg)	-	-	-	244x10^3

In order to analyze the behavior of the fluids under hydrodynamically fully developed and developing region, three different flow conditions were used. As shown in Table 3, different particle concentrations are assumed and the properties of bulk fluids calculated using equations (16), (17), (18) and (21) are shown in Table 4.

As shown in Table 3, three different flow conditions, one constant Re and two different mass flow rates are used. Since

the particle heat capacity as shown in equation (20) is temperature dependent, the following equation was used to calculate the bulk heat capacity of slurry (assuming the PCM starts to melt at the inlet and all the PCM is completely melt at the exit of the channel)

$$c_{p,bulk,2} = c_m\left(c_{p,pcm} + \frac{h_{sf}}{T_{Mr}}\right) + (1 - c_m)c_{p,f} \quad (25)$$

Table 3 Simulation Parameters

Flow and Heat Transfer Parameters	Value	Description
Q [W/cm^2]	500, 100	Heat flux
c	0, 0.1, 0.2, 0.25	Volume concentration
Re	50	Reynolds number
$\dot{m}$ [kg/s]	3.12x10^{-4}, 3.12x10^{-5}	Mass flow rate

Table 4 Properties of bulk fluids at different concentrations

Base fluid, c	ρ_{bulk} (kg/m^3)	$C_{pbulk,2}$ (J/kg.K)	k_{bulk} (W/m.K)	μ_{bulk} (Pa.s)	Pr
Water, c=0.1	974.7	5958.8	0.528	0.0013	15.16
Water, c=0.2	952.4	7820.8	0.462	0.0020	34.37
Water, c=0.25	941.25	8784.9	0.431	0.0026	53.95
Oil, c=0.1	855.9	4114.6	0.146	1.13	31.79 x10^3
Oil, c=0.2	846.8	6396.1	0.146	1.70	74.25 x10^3
Oil, c=0.25	842.25	7555.4	0.147	2.22	114.2 x10^3
PAO, c=0.1	782.1	4650.6	0.144	0.0060	193.29
PAO, c=0.2	781.2	7064.7	0.145	0.0090	440.24
PAO, c=0.25	780.75	8273.9	0.145	0.0118	670.64

The hydrodynamic entrance length (Le_D) and thermal entrance length (Le_T) for the fluids is shown in Table 5.

$$Le_D = 0.05ReD_h \quad (26)$$

$$Le_T = 0.05RePrD_h \quad (27)$$

It can be observed from the table that the flow can be considered hydrodynamically fully developed for all the cases, except for water at larger mass flow rate.

For all the cases used in the study, the flow is not thermally fully developed as shown by the Graetz number for the cases in Figure 4. In the figure, Graetz number is be calculated using equation (28):

$$Gz = \frac{D_h RePr}{x} \quad (28)$$

where $x = L = 0.01$m in Figure 4.

Table 5 Thermal Entrance lengths for slurries and base fluids for the parametric study

Fluid	$\dot{m}_1$ = 3.12x10^{-4} (kg/s)		$\dot{m}_2$ = 3.12x10^{-5} (kg/s)		Re = 50	
	Le_D (m)	Le_T (m)	Le_D (m)	Le_T (m)	Le_D (m)	Le_T (m)
Water, c=0	0.0150	0.104	0.0015	0.0104	0.0015	0.0104
Water, c=0.1	0.0112	0.169	0.00112	0.0169	0.0015	0.0227
Water, c=0.2	0.0074	0.254	0.00074	0.0254	0.0015	0.0516
Water, c=0.25	0.0057	0.306	0.00057	0.0306	0.0015	0.0809
Oil, c=0	1.79x10^{-5}	0.195	1.79x10^{-6}	0.0195	0.0015	16.3
Oil, c=0.1	1.33x10^{-5}	0.424	1.33x10^{-6}	0.0424	0.0015	47.7
Oil, c=0.2	8.83x10^{-6}	0.656	8.83x10^{-7}	0.0656	0.0015	111.4
Oil, c=0.25	6.77x10^{-6}	0.773	6.77x10^{-7}	0.0773	0.0015	171.3
PAO, c=0	3.37x10^{-3}	0.235	3.37x10^{-4}	0.0235	0.0015	0.1047
PAO, c=0.1	2.51x10^{-3}	0.485	2.51x10^{-4}	0.0485	0.0015	0.2899
PAO, c=0.2	1.66x10^{-3}	0.732	1.66x10^{-4}	0.0732	0.0015	0.6604
PAO, c=0.25	1.27x10^{-3}	0.854	1.27x10^{-4}	0.0854	0.0015	1.0060

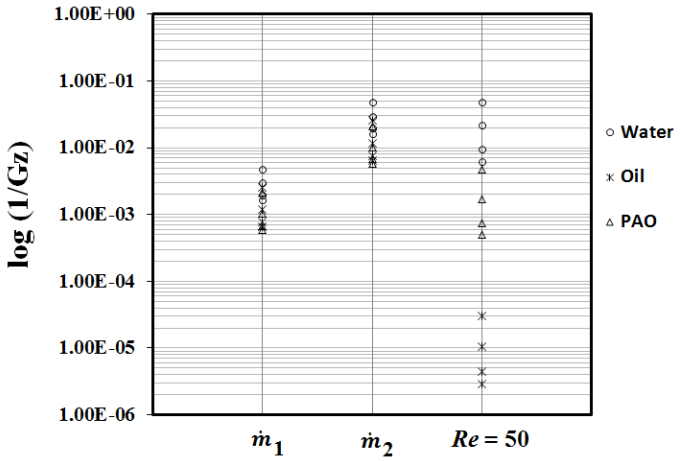

Figure 4: Log (Gz^{-1}) for the flow parameters used

NUMERICAL RESULTS

The pressure drop and bulk temperature rise are defined as in Equation (29), and the bulk mean outlet temperature of the fluid at the exit are calculated as in Equation (30):

$$\Delta P = p_{in} - p_{out};\ \Delta T = T_{in} - T_{out} \quad (29)$$

$$T_{out} = \frac{\int Tc_{p,b}(n,\vec{u})ds}{\int c_{p,b}(n,\vec{u})ds} \quad (30)$$

where *ds* is the surface area at the corresponding boundary (inlet for average pressure calculations and outlet for bulk mean temperature calculations). For the simulations, unstructured mesh was created using the default mesh option in COMSOL and the results were checked for grid independency. The results were found to satisfy the global energy balance at the inlet and outlet of the channel within 4% balance.

A. Hydrodynamic Performance

The pressure drop obtained for the three base fluids for the three flow conditions is shown in Table 5. Figures 5 to 7 show the pressure drop ratio (as defined in equation (31)) for the flow conditions used.

$$\Delta P_{ratio} = \frac{\Delta P_{slurry}}{\Delta P_{basefluid}} \quad (31)$$

From Table 5, it can be observed that the pressure drop of oil is larger for all the individual cases due to higher viscosity of the fluid. The pressure drop increase is larger when the case with constant *Re* is considered. Figures 5-7, show that the pressure drop increases with increase in particle concentration, as expected.

Table 5 Pressure drop for the base fluids

Flow Parameter	Base Fluid	Pressure Drop (pa)
$\dot{m}_1$=3.12x10^{-4} kg/s	Water	2.06x10^{3}
	Oil	7.05x10^{5}
	PAO	9.29x10^{3}
$\dot{m}_2$ =3.12x10^{-5} kg/s	Water	85.83
	Oil	7.05x10^{4}
	PAO	473.58
***Re* = 50** ($\dot{m}$ =3.13x10^{-7} kg/s for water, *c*=0) ($\dot{m}$ =2.63x10^{-4}kg/s for oil, *c*=0) ($\dot{m}$ =1.41x10^{-6}kg/s for PAO, *c*=0)	Water	85.83
	Oil	6.45x10^{7}
	PAO	2.92x10^{3}

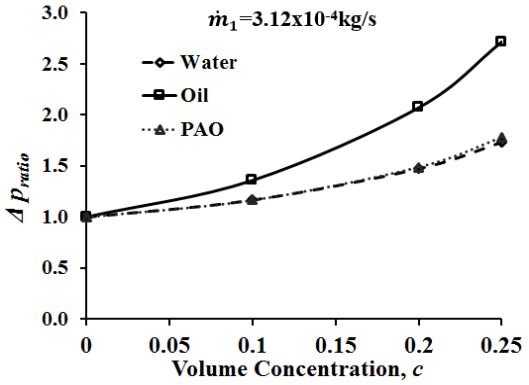

Figure 5 Pressure drop vs. concentration $\dot{m}_1$=3.12x10^{-4}kg/s

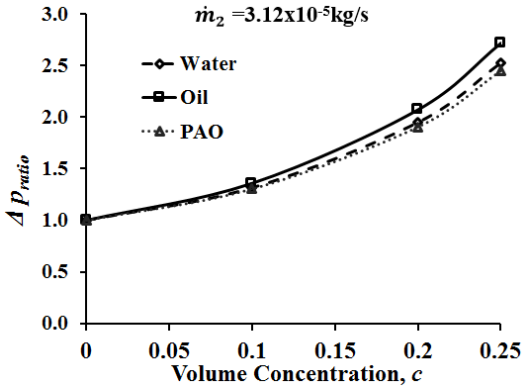

Figure 6 Pressure drop vs. concentration $\dot{m}_2$ =3.12x10^{-5}kg/s

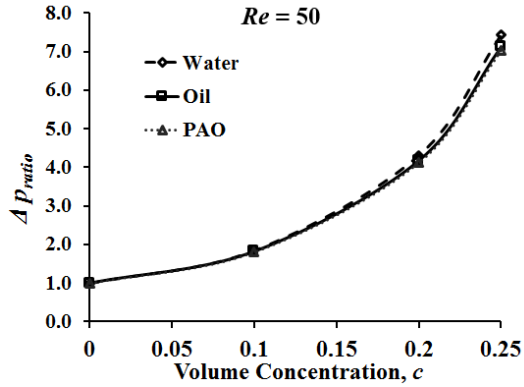

Figure 7 Pressure drop vs. concentration *Re* = 50

From Figure 5 it can be inferred that the variation in pressure drop ratio for water is higher for $\dot{m}_1$ compared to the variation in PAO and oil. This could be due to the hydrodynamically developing flow in case of water. For the remaining two fluids, the flow is fully developed at the larger mass flow rate. From Figure 6, it can be observed that the variation in pressure drop ratio at different concentrations for all the three fluids is slightly different, but due to the fully developed nature of the flow, the variation for water is not as much. From Figures 6 and 7 it can be observed that the increase in pressure drop with particle concentration is larger for constant *Re* case compared constant mass flow rate.

B. Thermal Performance

All the numerical results are based on the same mass flow rate and same inlet temperature T_{in} =296.9K. Two different mass flow rates were used $\dot{m}_1$ =3.12x10^{-4}kg/s and $\dot{m}_2$ =3.12x10^{-5}kg/s. For larger flow rate, a heat flux of 500 W/cm^2 was used. For lower flow rate and constant Re cases, a heat flux of 50 W/cm^2 was used. It should be noted that the temperature rise in the slurry would depend on the amount of PCM melted and hence, the bulk temperature rise may not be the same. The

heat transfer performance was evaluated using the heat transfer coefficient defined as:

$$h = \frac{q}{(T_{w,\max} - T_{in})} \tag{32}$$

$T_{w,max}$ is the maximum wall temperature at the heater. The Nusselt number ratio defined as in Equation (33) is shown in Figures 8 to 10. It can be observed that though the ratio of heat flux and mass flow rate is kept constant for both the cases, the increase in Nu_{ratio} is larger for lower mass flow rate suggesting the importance of thermal development length.

$$Nu_{ratio} = \frac{Nu_{slurry}}{Nu_f} \tag{33}$$

The *Nu* for each fluid is defined as in equation.

$$Nu = \frac{hD_h}{k} \tag{34}$$

For all the cases, Nusselt number ratio increases with increase in particle volume concentration. The Nu_{ratio} for all the three fluids is larger at $\dot{m}_2$ compared to $\dot{m}_1$. The Nu_{ratio} is highest for constant *Re* cases for all the fluids. Water has the highest ratio and increases faster than oil and PAO. For example, if the cases with *c*=0.25 are considered (shown Table 6), the Nu_{ratio} for water is higher for each case compared to PAO and oil, suggesting the thermal conductivity importance in heat transferred. In case of both PAO and oil, the variation in thermal conductivity is not as much due to the presence of PCM, whereas for water, the decrease in thermal conductivity affects the Prandtl number which in turn affects the Nusselt number. If the individual *Nu* is considered for constant *Re*, oil has the highest *Nu* (as shown in Figure 11) due to the high *Pr* of the fluid.

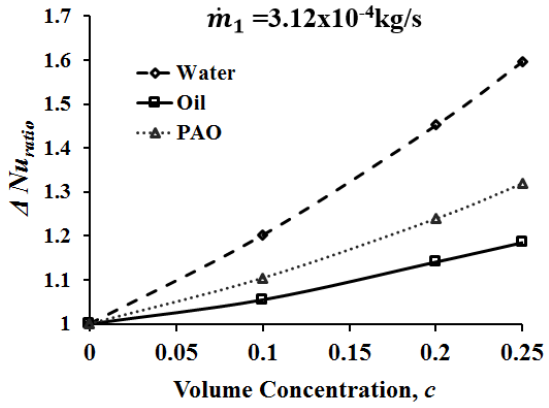

Figure 8 Nu_{ratio} for $\dot{m}_1$ =3.12x10^{-4}kg/s

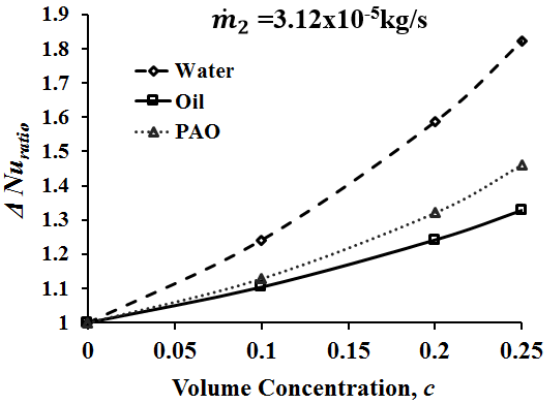

Figure 9 Nu_{ratio} for $\dot{m}_2$ =3.12x10^{-5}kg/s

Table 6 Nu_{ratio} for slurries at *c*=0.25

Flow Parameter	Base Fluid	Nu_{ratio}
$\dot{m}_1$=3.12x10^{-4}kg/s	Water	1.59
$\dot{m}_1$=3.12x10^{-4}kg/s	Oil	1.18
$\dot{m}_1$=3.12x10^{-4}kg/s	PAO	1.32
$\dot{m}_2$ =3.12x10^{-5}kg/s	Water	1.82
$\dot{m}_2$ =3.12x10^{-5}kg/s	Oil	1.32
$\dot{m}_2$ =3.12x10^{-5}kg/s	PAO	1.46
***Re* = 50**	Water	5.48
***Re* = 50**	Oil	1.37
***Re* = 50**	PAO	4.23

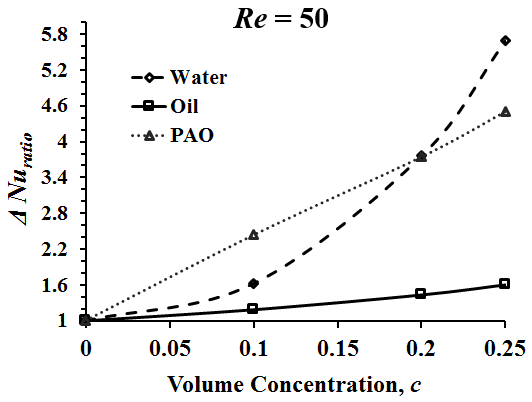

Figure 10 Nu_{ratio} for *Re* = 50

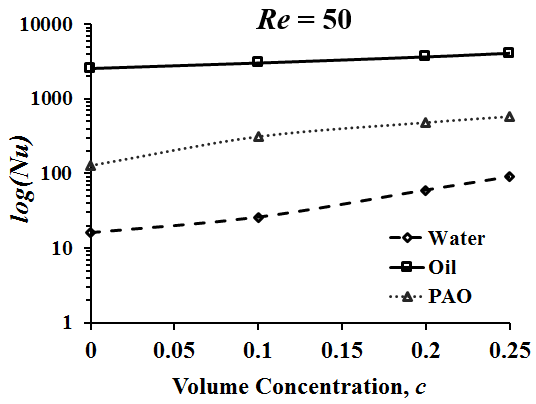

Figure 11 Nusselt number for *Re* = 50

D. Performance Factor (PF)

The combined thermal and hydrodynamic performance is analyzed by estimating the performance factor (*PF*) which is calculated using equation (35).

$$Performance\ factor, PF = \left(\frac{h_{slurry}}{h_{basefluid}}\right)/\left(\frac{\Delta P_{slurry}}{\Delta P_{basefluid}}\right) \quad (35)$$

It can be observed from Figures 12 and 13 that for constant mass flow rate cases, the *PF* is less than 1, suggesting the performance of slurry is lower compared to their base fluid. When the performance of all the three liquids is compared, the *PF* of PAO is highest, which could be due to the lower viscosity compared to oil and thermal conductivity is not lowered as much when compared to water *PF*. Though there is no degradation of thermal conductivity for oil with the addition of EPCM particles, the viscosity increase is much larger factor. Hence *PF* of oil is lowest compared to PAO and water at any concentration. Though the Nu_{ratio} is larger for water, the *PF* factor is lower than PAO.

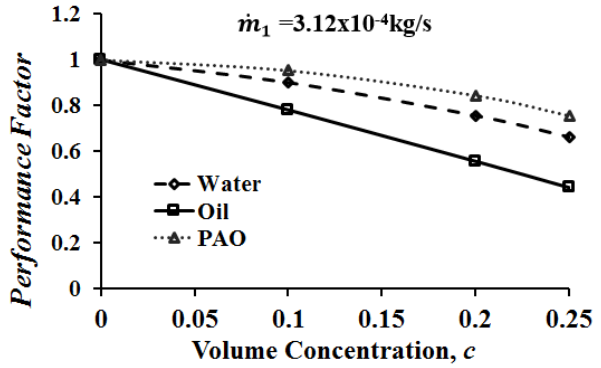

Figure 12 Performance Factor for $\dot{m}_1$ =3.12x10^{-4}kg/s

From Figure 14, it can be observed that *PF* is greater than 1 for constant *Re* for a particle concentration of 0.1 with PAO as the base fluid and for all other cases, *PF* is lower than 1. As the particle concentration increased, the increase in viscosity affected the *PF*. The exceptional case of PAO at *c* = 0.1 can be due to the large increase Nusselt number but not as much increase in the pressure drop at that concentration.

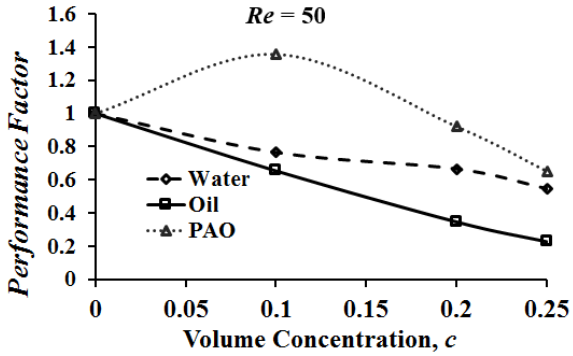

Figure 14 Performance Factor for *Re* = 50

In case of microchannels, due to the fixed length of channels, improving the heat capacity of the fluids by adding EPCM particles is not always advantageous, since the flow may not be thermally fully developed and the increase in viscosity can be larger than the improvement in heat transfer performance. As can be observed from the results, for the cases where the thermal developing length is an order of magnitude larger than the length of the channel, base fluids always performed better compared to slurry flows, even when the thermal conductivity of base fluid is comparable to that of base fluid. Though engine oil has the same thermal conductivity as PCM, the overall performance is not high for slurry due to the very high Prandtl number. Hence, using PCM slurry is advantageous only if the base fluids have low viscosity and thermal conductivity (such as PAO).

CONCLUSION

The performance of three different types of encapsulated phase change material slurries is investigated under constant mass flow rate and *Re* conditions in thermally developing regime. The following conclusions can be drawn from the study.

[1] The thermal performance of slurries is larger for constant *Re* condition than constant mass flow rate condition for any fluid.

[2] *PF* of base fluids is larger than slurries for both the cases where constant mass flow rate condition is used. The increase in pressure drop dominates the increase in heat transfer enhancement due to presence of PCM particles.

[3] The *Nu* for oil is the largest due to high *Pr*, however, when the Nu_{ratio} is considered, water performs better.

[4] The *PF* of PAO is higher for all the cases, suggesting that both thermal conductivity and viscosity are important to consider when slurry flow is considered in microchannels, where the flow mostly in thermally developing regime.

[5] The *PF* of PAO is greater than 1 for the constant *Re* condition. An optimum volume concentration for PAO in microchannels is 0.1.

From the study it can be concluded that in case of microchannel flows, since the length of microchannel is limited, utilizing PCM slurry is advantageous if the heat transfer fluid being used has low viscosity and equal or lower thermal conductivity than PCM material.

REFERENCES

[1] Tuckerman, D.B. and Pease, R.F.W., High-Performance Heat sinking for VLSI, *IEEE. Electronic Device Letters*, vol. EDL-2, 1981, pp. 126-129.

[2] Copeland, D., 1995, Manifold Microchannel Heat Sinks: Analysis and Optimization, *Therm. Sci. Eng.*, 3(1), pp. 7–12.

[3] Copeland, D., Behnia, M., and Nakayama, W., 1998, Manifold Microchannel Heat Sinks: Conjugate and Extended Models, *International Journal of Microelectronic Packaging, Materials and Technologies*, 1(2), pp. 139–152.

[4] S. Kuravi, J. Du, L. Chow, Encapsulated Phase Change Material Slurry Flow in Manifold Microchannels, *Journal of Thermophysics and Heat Transfer*, vol: 24, No.2, pp: 364-373, 2010.

[5] S. Kuravi, K. Kota, J. Du, L. Chow, Numerical Investigation of Flow and Heat Transfer Performance of Nano-Encapsulated Phase Change Material (NEPCM) Slurry in Microchannels, *Journal of Heat Transfer*, vol: 131, pp: 062901(1-9), 2009.

[6] S. Kuravi, J. Du, Louis Chow, Encapsulated Phase Change Material Slurry Flow in Manifold Microchannles, *presented at 41st AIAA Thermophysics Conference*, San Antonio, Texas, June 22 – 25, 2009.

[7] S. Kuravi, K. Kota, J. Du, L. Chow, David Colvin, Numerical Simulation of Heat Transfer in a Microchannel Heat Sink With Micro Encapsulated Phase Change Material (MEPCM) Slurry, *presented at Proceedings of ASME-JSME Thermal Engineering Summer Heat Transfer Conference, Vancouver*, Canada, July 8 – 12, 2007.

[8] J. Y. Jung, H. S. Oh, and H. Y. Kwak, Forced convective heat transfer of nanofluids in microchannels, *International Journal of Heat and Mass Transfer*, vol. 52, no. 1-2, pp. 466–472, 2009.

[9] L. Gong, K. Kota, W. Tao, Y. Joshi, Parametric Numerical Study of Flow and Heat Transfer in Microchannels with Wavy Walls, *Journal of Heat Transfer*, vol. 133, No. 5, 051702 (1-10), 2011.

[10] L. Gong, K. Kota, W. Tao, Y. Joshi, Thermal Performance of Microchannels with Wavy Walls for Electronics Cooling, Components, Packaging and Manufacturing Technology, *IEEE Transactions*, vol. 1, No. 7, pp. 1029-1035, 2011.

[11] K. Kota, L. Gong, W. Tao, Y. Joshi, Effect of Wall Roughness on Thermal Performance of Wavy Microchannels, *presented at The 10th International Workshop on Micro and Nanotechnology for Power Generation and Energy Conversion Applications*, Leuven, Belgium, November 30-December 3, 2010.

[12] D. Sharma, H. Garg, P. P. Singh, and V. Karar, Numerical Study on the Performance of Double Layer Microchannel with Liquid Gallium and Water, *Advances in Mechanical Engineering*, vol. 2013, Article ID 324578, 15 pages, 2013.

[13] K. Ma and J. Liu, Liquid metal cooling in thermal management of computer chips, *Frontiers of Energy and Power Engineering in China*, vol. 1, no. 4, pp. 384–402, 2007.

[14] K. Q. Ma and J. Liu, Nano liquid-metal fluid as ultimate coolant, *Physics Letters Section A*, vol. 361, no. 3, pp. 252–256, 2007.

[15] T. Li, Y. G. Lv, J. Liu, and Y. X. Zhou, A powerful way of cooling computer chip using liquid metal with low melting point as the cooling fluid, *Forschung im Ingenieurwesen*, vol. 70, no. 4, pp. 243–251, 2006.

[16] Peijie Li, Sarada Kuravi, "Comparative Study of Thermal Performance of Liquid Metal and Water Flow through a Minichannel", *presented at Proceedings of International Conference on Research and Innovations in Mechanical Engineering (ICRIME 2013)*, Ludhiana, India, October 24-26, 2013.

[17] K. Chen, and M. M. Chen, An analytical and experimental investigation of the convective heat transfer of phase change slurry flows, *Ziejiang University Press*, China, 2: 496-501, 1987.

[18] S. Sengupta, Microencapsulated phase change material slurries for thermal management of electronic packages, Dept. of Mech. Eng., Univ. of Miami, *Quarterly report submitted to Florida High Technology and Industrial Council*, 1988.

[19] D.P. Colvin, Y.B. Bryant, J.C. Mulligan and J.D. Duncan, Microencapsulated phase change heat transfer system, *WRDC-TR-89-3072*, U.S. Air Force Wright R & D center, OH, 1989.

[20] K.E. Kasza, M.M. Chen, Improvement of the performance of solar energy or waste heat utilization systems by using phase-change slurry as an enhanced heat transfer storage fluid, *Journal of Solar Energy Engineering*, 107: 229-236, 1985.

[21] S.K. Roy and S. Sengupta, An evaluation of phase change microcapsules for use in enhanced heat transfer fluids, *International Communication of Heat and Mass Transfer*, 18 (4): 495-507, 1991.

[22] M. Goel, S.K. Roy and S. Sengupta, Laminar forced convection heat transfer in microcapsulated phase change material suspension, *Int. J. Heat Mass Transfer*, 37: 593-604, 1994.

[23] P. Charunyakorn, S. Sengupta, S.K. Roy, Forced convection heat transfer in microencapsulated phase change material slurry: *flow in circular ducts, Int. J. Heat Mass Transfer*, 34: 819-833, 1991.

[24] Y.W. Zhang, and A. Faghri, Analysis of forced convection heat transfer in microcapsulated phase change material suspensions. *J Thermophysics Heat Transfer*, 9 (4): 727–732, 1995.

[25] Y. Yamagishi, H. Tahkeuchi, A. Pyatenko and N. Kayukawa, A Technical evaluation of a microencapsulated PCM slurry as a heat transfer fluid, *AICHE Journal*, 45(4): 696-707, 1999.

[26] E.L. Alisetti, and S. K. Roy, Forced convection heat transfer to phase change material slurries in circular ducts, J. *Thermophysics Heat Transfer*, 14: 115-118, 2000.

[27] Y. Zhang, X. Hu, and X. Wang, Theoretical analysis of convective heat transfer enhancement of microencapsulated phase change material slurries. *Heat and Mass Transfer*, 40: 59-66, 2003.

[28] Y.L.Hao and Y.-X. Tao, A numerical model for phase-change suspension flow in microchannels, *Numerical Heat transfer A*, 46: 55-77, 2004.

[29] K.Q. Xing, Y.-X. Tao and Y.L. Hao, Performance evaluation of liquid flow with PCM particles in microchannels, *J. Heat Transfer*, 127: 931-940, 2005.

[30] A. Karnis, H. L. Goldsmith, S. G. Mason, The kinetics of flowing dispersions. I. Concentrated suspensions of rigid particles, *J. Colloid. Interf. Sci.*, 22: 531–553, 1966.

[31] R.W. Watkins, C. R. Robertson, and A. Acrivos, Entrance region heat transfer in flowing suspensions, *Int. J. Heat Mass Transfer*, 19: 693-695, 1976.

[32] S. T. Wereley and C. D. Meinhart, Micron-resolution particle image velocimetry, In: K. S. Breuer ed., Micro-and nano-scale diagnostic techniques, Springer Verlag, New York, 2005.

[33] V. Vand, Theory of viscosity of concentrated suspensions, Nature, 155: 364-365, 1945.

[34] V. Vand, Viscosity of solutions and suspensions, J. Phys. Coll. Chem.,52: 300-321, 1948.

[35] Sarada Kuravi, Jamie Trahan, Muhammad Rahman, Yogi Goswami, Elias Stefanakos, "Analysis of transient heat transfer in a thermal energy storage module", *ASME 2010 International Mechanical Engineering Congress and Exposition*, Vancouver, British Columbia, November 12 – 18, 2010.